



APPLICATION OF ADAPTIVE VARIABLE SPEED BACK-STEPPING SLIDING MODE CONTROLLER FOR PMLSM POSITION CONTROL

Mei-Yung Chen

Department of Mechatronic Engineering, National Taiwan Normal University, Taipei City, Taiwan, R.O.C,
cmy@ntnu.edu.tw

Jian-Shiun Lu

Department of Mechatronic Engineering, National Taiwan Normal University, Taipei City, Taiwan, R.O.C

Follow this and additional works at: <https://jmstt.ntou.edu.tw/journal>



Part of the [Controls and Control Theory Commons](#)

Recommended Citation

Chen, Mei-Yung and Lu, Jian-Shiun (2014) "APPLICATION OF ADAPTIVE VARIABLE SPEED BACK-STEPPING SLIDING MODE CONTROLLER FOR PMLSM POSITION CONTROL," *Journal of Marine Science and Technology*. Vol. 22: Iss. 3, Article 13.

DOI: 10.6119/JMST-014-0102-1

Available at: <https://jmstt.ntou.edu.tw/journal/vol22/iss3/13>

This Research Article is brought to you for free and open access by Journal of Marine Science and Technology. It has been accepted for inclusion in Journal of Marine Science and Technology by an authorized editor of Journal of Marine Science and Technology.

APPLICATION OF ADAPTIVE VARIABLE SPEED BACK-STEPPING SLIDING MODE CONTROLLER FOR PMLSM POSITION CONTROL

Mei-Yung Chen and Jian-Shiun Lu

Key words: permanent magnet iron core linear synchronous motor, adaptive variable speed back-stepping sliding mode controller, high-precision servo positioning platform.

ABSTRACT

In this research, an adaptive variable speed back-stepping sliding mode controller (AVSBSMC) is proposed to control the permanent magnet linear synchronous motor (PMLSM) on high-precision positioning servo system platform. This controller combines the dynamic features of variable speed control (VSC) and the positioning characteristics of adaptive back-stepping sliding mode control (ABSMC). Firstly, the detailed dynamic machine model of PMLSM is established. Secondly, the proportional-integral-derivative (PID) and ABSMC controllers are proposed to compensate the uncertainties in position control. Then, the one provides the better servo performances is the position controller in the motor system. Thirdly, the variable speed controller (VSC) and each segment of the variable speed sliding functions are designed to combine with the ABSMC controller. Switching control is then used to change the system control mode accomplishing the high-precision positioning control. Our experimental results demonstrate that the AVSBSMC enhance the positioning accuracy of linear motor and reduce the transient overshoot effectively.

I. INTRODUCTION

Because of development of industry, the use of a linear motor as driving power source has been increasing. The permanent magnetic linear synchronous motor (PMLSM) provides several advantages, such as 1) high-speed drive, 2) powerful thrust, 3) a long driving stroke, 4) no backlash effect, 5) direct driving mechanical construction, 6) high repeatability,

and 7) excellent servo response. These features indicate that the PMLSM is ideal for use with the servo system, such as X-Y positioning platforms, the transmission equipment for industrial robots, power equipment in the semiconductor industry, and servo systems in the automation industry, which is required for high-precision performance. Therefore, a PMLSM was used as the driving power source for an X-Y high-precision linear positioning platform in this study.

Although the dynamic response of the driving performance of the PMLSM is excellent, the positioning and tracking performances of the PMLSM are adversely affected by numerous nonlinear disturbances and noises, such as 1) the friction force of the linear rail, 2) ripple effect between the magnetic poles and air gap, 3) load effect on the carrier, 4) vibrations in the platform mechanism, and 5) variation of the system parameters.

Zschaeck *et al.* [16] combined a bristle model with a disturbance observer to compensate for the force of friction and restrain the disturbances of nonlinear friction force to improve system accuracy. Chen *et al.* [5] used hysteretic relay, which is a feedback component in system identification technology, to establish a model of the ripple effect between magnetic poles. This model was then compensated and enhanced by using system dynamic responses. Cao and Low [3] designed a repetitive model predictive controller (MPC) to increase the robustness of the system and reduce disturbances in tracking performance from the load effect. Bianchini *et al.* [1] analyzed the relative relationship between the frequency and amplitude of vibration in the linear guideway. Mechanic vibration is caused by nonuniform thrust and the load effect. Butcher and Karimi [2] designed the iterative learning control algorithm to estimate the system parameters and analyzed the trends in system variation to improve the stability and robustness of the control system. The aforementioned materials are used for improving the performance of positioning platforms.

II. SYSTEM MODEL OF PMLSM

1. The Structure of PMLSM and Its Driving Principles

The structure of PMLSM can be regarded as a rotary motor

Paper submitted 08/20/12; revised 02/17/13; accepted 01/02/14. Author for correspondence: Mei-Yung Chen (e-mail: cmy@ntnu.edu.tw).

Department of Mechatronic Engineering, National Taiwan Normal University, Taipei City, Taiwan, R.O.C.

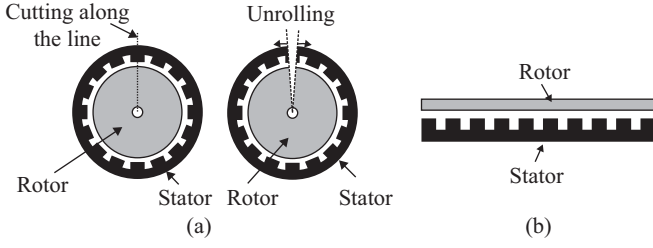


Fig. 1. The structures of (a) Rotary motor, (b) Linear motor.

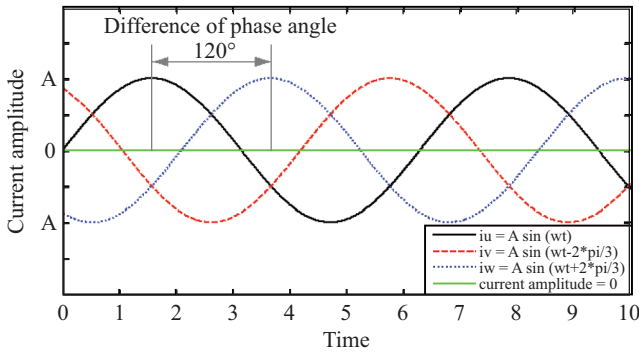


Fig. 2. The three-phase sinusoidal current.

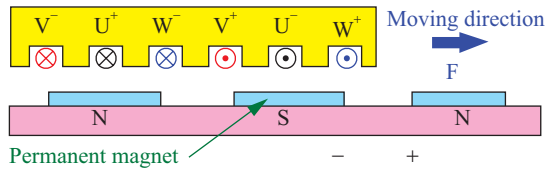


Fig. 3. The source of electromagnetic force.

which is cut by a radial plane and is unrolled. It includes a rotor, a stator and the air gap. The concept of design is shown in Fig. 1 [4].

The actuation principle of the PMLSM is similar to a rotary motor. In the driving system, the pulse wide modulation (PWM) and inverter were employed to generate the sinusoidal current signals i_n , $n \in u, v, w$. The differences of current phase angle between each wave are 120° which are shown in Fig. 2. The system utilizes three-phase current to generate the electromagnetic field. Electromagnetic force F is emerged then by the changing of magnetic field between three-phase current coils and the permanent magnet stator. The symbols of U, V and W represent the power lines of PMLSM transmitting the three-phase current in system, shown in Fig. 3.

According to the above analysis, the electromagnetic force F can be expressed as Eq. (1).

$$F = \rho \cdot I \cdot l \cdot B_{pmf} \quad (1)$$

where ρ is the turns per coil, I is the three-phase current vectors, l is the length of coil in permanent magnet field and B_{pmf} is the intensity of permanent magnet field.

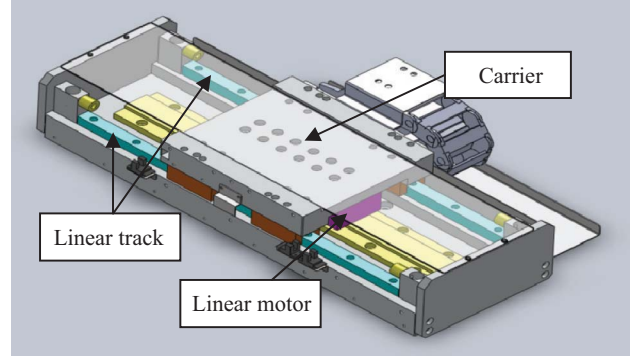


Fig. 4. The structure of PMLSM.

The electromagnetic force F actuates the carrier moving along a linear direction. The structure of PMLSM is shown in Fig. 4.

2. Mathematical Model of Electromagnetic Force

The voltage and current vectors of the PMLSM in matrix form are expressed as follow [7].

$$V_{abc} = r_s \cdot I_{abc} + \frac{d}{dt} \lambda_{abc} \quad (2)$$

$$\lambda_{abc} = L_s \cdot I_{abc} + \lambda_{\max} \quad (3)$$

where

$$V_{abc} = [v_{as} \quad v_{bs} \quad v_{cs}]^T, \quad I_{abc} = [i_{as} \quad i_{bs} \quad i_{cs}]^T,$$

$$\lambda_{abc} = [\lambda_{as} \quad \lambda_{bs} \quad \lambda_{cs}]^T, \quad r_s = r \cdot I_{3 \times 3} \text{ (unit matrix),}$$

$$\lambda_{\max} = \left[\sin\left(\frac{\pi x}{\tau}\right) \quad \sin\left(\frac{\pi x}{\tau} - \frac{2\pi}{3}\right) \quad \sin\left(\frac{\pi x}{\tau} + \frac{2\pi}{3}\right) \right]^T$$

$$L_s =$$

$$\begin{bmatrix} L_{ls} + L_A - L_B \cos\left(\frac{2\pi x}{\tau}\right) & -\frac{1}{2}L_A - L_B \cos 2\left(\frac{\pi x}{\tau} - \frac{\pi}{3}\right) & -\frac{1}{2}L_A - L_B \cos 2\left(\frac{\pi x}{\tau} + \frac{\pi}{3}\right) \\ -\frac{1}{2}L_A - L_B \cos 2\left(\frac{\pi x}{\tau} - \frac{\pi}{3}\right) & L_{ls} + L_A - L_B \cos 2\left(\frac{\pi x}{\tau} - \frac{2\pi}{3}\right) & -\frac{1}{2}L_A - L_B \cos 2\left(\frac{\pi x}{\tau} + \pi\right) \\ -\frac{1}{2}L_A - L_B \cos 2\left(\frac{\pi x}{\tau} + \frac{\pi}{3}\right) & -\frac{1}{2}L_A - L_B \cos 2\left(\frac{\pi x}{\tau} + \pi\right) & L_{ls} + L_A - L_B \cos 2\left(\frac{\pi x}{\tau} + \frac{2\pi}{3}\right) \end{bmatrix}$$

where V_{abc} , I_{abc} , λ_{abc} are the vectors of phase voltages, currents, and flux linkages. r_s is the resistance matrix of primary winding. Then L_{ls} is the leakage inductance, τ is pole pitch, x is the position of carrier, and λ_{\max} is the amplitude of sinusoidal flux linkages in primary windings.

We selected process which mathematically replaces the abc stator coils by fictitious qdo coils fixed to the translator to facilitate the analysis to the system, shown as follow.

$$v_q = ri_q + \frac{d}{dt}\lambda_q + w\lambda_d \tag{4}$$

$$v_d = ri_d + \frac{d}{dt}\lambda_d - w\lambda_q \tag{5}$$

$$v_o = ri_o + L_{ls}\dot{i}_o \tag{6}$$

where

$$\lambda_d \equiv L_d i_d + \sqrt{\frac{2}{3}}\lambda_{\max}, \quad \lambda_q \equiv L_q i_q, \quad w = \frac{\pi}{\tau}\dot{x}$$

$$L_d \equiv L_{ls} + L_A + \frac{3}{2}L_B, \quad \text{and} \quad L_q \equiv L_{ls} - L_A - \frac{3}{2}L_B$$

To supply an ideal three-phase AC power to the system, the v_o and i_o are zero after d - q axes transformation.

$$v_o = 0 \tag{7}$$

$$i_o = 0 \tag{8}$$

For a magnetically linear field, and neglecting copper, hysteresis and eddy current losses, the electromagnetic force F_e can be simplified as shown in Eq. (9).

$$F_e = \frac{\pi}{\tau} \left[(L_d - L_q) \cdot i_q i_d + \sqrt{\frac{2}{3}} \cdot i_q \cdot \lambda_{\max} \right] \tag{9}$$

3. Dynamical System Model of PMLSM

According to the above deduction, the dynamical system model of PMLSM can be expressed as Eqs. (10)~(13) [4].

$$\frac{dx}{dt} = \dot{x} = v \tag{10}$$

$$\frac{dv}{dt} = \ddot{x} = \frac{1}{M}(-Bv + F_e - F_L) \tag{11}$$

$$\frac{di_q}{dt} = \frac{1}{L_q} \left(-ri_q - \frac{\pi}{\tau}\dot{x}L_d i_d - \sqrt{\frac{2}{3}}\frac{\pi}{\tau}\dot{x}\lambda_{\max} + v_q \right) \tag{12}$$

$$\frac{di_d}{dt} = \frac{1}{L_d} \left(-ri_d + \frac{\pi}{\tau}\dot{x}L_q i_q + v_d \right) \tag{13}$$

where M is the mass of carrier, B is the viscous friction coefficient, and F_L is the uncertain forces caused by friction, load effect, ripple effect, and other uncertain noises.

To integrate Eqs. (12) and (13), the dynamic equation of d - q axes current in matrix form can be expressed as Eq. (14).

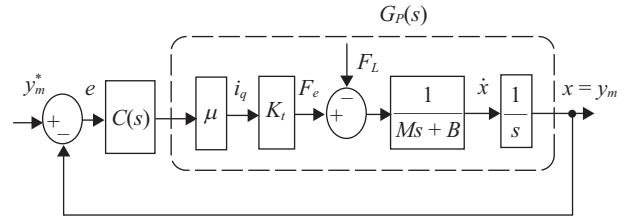


Fig. 5. Block diagram of simplified closed-loop system.

$$\begin{bmatrix} \dot{i}_d \\ \dot{i}_q \end{bmatrix} = \begin{bmatrix} -\frac{r}{L_d} & 0 \\ 0 & -\frac{r}{L_q} \end{bmatrix} \cdot \begin{bmatrix} i_d \\ i_q \end{bmatrix} + \begin{bmatrix} \frac{1}{L_d}(v_d + wL_q i_q) \\ \frac{1}{L_q}(v_q - wL_d i_d - \sqrt{\frac{2}{3}}w\lambda_{\max}) \end{bmatrix} \tag{14}$$

To decouple the control system into working at linearly independent condition, the control voltage vector v^* is defined by Eq. (15). Finally, the uncoupled system is derived as Eq. (16).

$$v^* = \begin{bmatrix} v_d^* \\ v_q^* \end{bmatrix} = \begin{bmatrix} v_d + wL_q i_q \\ v_q - wL_d i_d - \sqrt{\frac{2}{3}}w\lambda_{\max} \end{bmatrix} \tag{15}$$

$$\begin{bmatrix} \dot{i}_d \\ \dot{i}_q \end{bmatrix} = \begin{bmatrix} -\frac{r}{L_d} & 0 \\ 0 & -\frac{r}{L_q} \end{bmatrix} \cdot \begin{bmatrix} i_d \\ i_q \end{bmatrix} + \begin{bmatrix} \frac{1}{L_d} \cdot v_d^* \\ \frac{1}{L_q} \cdot v_q^* \end{bmatrix} \tag{16}$$

From the mathematical model and the uncoupled model of PMLSM, the simplified closed loop block diagram is shown in Fig. 5. Where y_m^* and y_m are the reference command and real position respectively. Moreover, the $G_p(s)$ is the controlled system, $C(s)$ is the position controller, and μ is constant of current control loop.

III. CONTROLLER DESIGN

The design processes of the system controllers are introduced in this section: to design the PID controller and ABSMC, then compare the two controllers in dynamic responses.

1. The Controller Design Process of PID

The PID controller has been widely used in industry because of its simple structures and high reliability. In contrast, the transient responses of system, the ability to resist the parameters variation and the robustness of against the load disturbances exhibit poor performances.

To avoid non-linear disturbances prior to the controllers

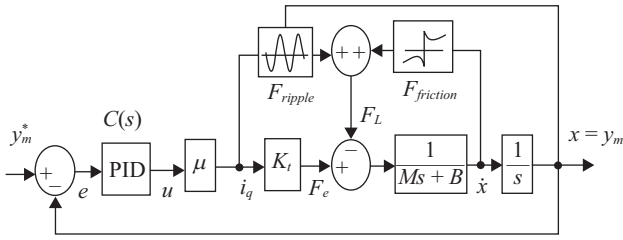


Fig. 6. Block diagram of PID control system.

design, the system control block diagram of PID controller is shown in Fig. 6, and the dynamic equation of control system can be expressed as Eq. (17).

$$M\ddot{x} + B\dot{x} = F_e - F_L - F_{ripple} - F_{friction} \quad (17)$$

$$F_{ripple} = R \cdot \sin(wx + \varphi) = R_c \cos(wx) + R_s \sin(wx) \quad (18)$$

$$F_{friction} = F_c \operatorname{sgn}(\dot{x}) + (F_s - F_c) e^{-\left(\frac{v}{v_s}\right)^2} \operatorname{sgn}(v) + B\dot{x} \quad (19)$$

where F_{ripple} is the ripple force and R, w, φ, R_c, R_s are the constants of system. $F_{friction}$ is the friction force. And F_s is maximum static friction force. F_c is coulomb friction force. And v_s is the speed parameter of Stribeck model.

However, $G_p(s)$ represent the nominal model of PMLSM, its transfer function is expressed as Eq. (20). And the mathematical model of PID is $C(s)$ presented as Eq. (21).

$$G_p(s) = \frac{\mu \cdot K_t}{M s^2 + (B + \mu \cdot K_t) s} \quad (20)$$

$$C(s) = K_p + \frac{K_I}{s} + K_D \cdot s \quad (21)$$

where K_p is the proportional gain constant, K_I is the integral constant, and K_D is the derivative constant.

By adjusting the three control parameters in on-line ways, it can improve the properties of PID controller and promote the positioning precisions and reduce the tracking errors synchronously of PMLSM control system.

2. The Controller Design Process of ABSMC

When PMLSM is in operation, the nonlinear external uncertainties disturb the control system, for instance, the friction of linear rails, the vibrations around motor, and the load effect. All these factors lead to the inaccurate system parameters and poor control accuracy. Therefore, ABSMC is used to reduce or even eliminate the external interferences in this research [6, 8, 10].

ABSMC controller integrates the design concepts of adaptive control law and robust control to avoid potential external disturbances and some unknown noises.

Refer the above Eqs. (10) and (11) in defining the system state variable $X_1 = x, X_2 = \dot{x}$ and reference input command y_d as well as taking into considerations of some effects of system parameters variation, external interferences thrust and the friction force in system model. The state variables can be defined as $X_1 = x = y_m, X_2 = \dot{x} = v, U = i_q$, and the state space model of PMLSM control system can be expressed as Eqs. (22)~(24).

$$\dot{X}_1 = X_2 \quad (22)$$

$$\dot{X}_2 = (A_m + \Delta A)X_2 + (B_m + \Delta B)U + C_m(F_L + F_{ripple} + F_{friction}) \quad (23)$$

$$Y = X_1 = y_m \quad (24)$$

where $A_m = -B/M, B_m = K_t/M, C_m = -1/M$. The ΔA and ΔB are uncertain parameters variation of M and B in the system. U is the control input i_q . Then to deduce Eq. (23) to Eqs. (25) and (26). D represents the quantity of system uncertain disturbances and some noises. Using the adaptive estimator to estimate D and assume that the estimated value is a constant during the estimation period.

$$\dot{X}_2 = A_m X_2 + B_m U + D \quad (25)$$

$$D = \Delta A X_2 + \Delta B U + C_m(F_L + F_{ripple} + F_{friction}) \quad (26)$$

The purpose of the control object is to make the response of the system output, $Y = y_m$, to tracing of the input command, $Y_d = y_m^*$ and achieving of the position tracking control. The steps of controller design are described below:

Step 1:

In order to control the tracking response, a function of position tracking error z_1 is defined as Eq. (27) and derivatized to Eq. (28). Then defined a stable function α_1 as shown in Eq. (29), a Lyapunov function V_1 in Eq. (30), and the second system variable z_2 in Eq. (31). Finally, by taking a derivative of Lyapunov function V_1 with time and integrate the above equations, the first equation about stability in system is derived (Eq. (32)).

$$z_1 = Y - Y_d \quad (27)$$

$$\dot{z}_1 = X_2 - \dot{Y}_d \quad (28)$$

$$\alpha_1 = c_1 z_1 \quad (29)$$

where c_1 is a positive constant.

$$V_1 = \frac{1}{2} z_1^2 \quad (30)$$

$$z_2 = X_2 - \dot{Y}_d + \alpha_1 \tag{31}$$

$$\dot{V}_1 = z_1(X_2 - \dot{Y}_d) = z_1(z_2 - \alpha_1) = z_1z_2 - c_1z_1^2 \tag{32}$$

Step 2:

Assume that the amount of the disturbances D satisfies the matching condition and value is bounded ($|D| \leq D_{max}$). Then take derivative of variable z_2 and expand it to Eq. (33). And next step is to define a second Lyapunov function V_2 as Eq. (34) in system which contains a sliding surface σ as Eq. (35).

$$\dot{z}_2 = \dot{X}_2 - \ddot{Y}_d + \dot{\alpha}_1 = A_m X_2 + B_m U + D - \ddot{Y}_d + \dot{\alpha}_1 \tag{33}$$

$$V_2 = V_1 + \frac{1}{2} \sigma^2 \tag{34}$$

$$\sigma = k_1 z_1 + z_2 \tag{35}$$

To take a derivative of the Lyapunov function V_2 and integrate the above functions Eqs. (32) and (33), then the second equation about stability in control system is derived as Eq. (36). The input control U of this equation can be defined as Eq. (37).

$$\begin{aligned} \dot{V}_2 &= \dot{V}_1 + \sigma \dot{\sigma} \\ &= z_1 z_2 - c_1 z_1^2 + \sigma(k_1 \dot{z}_1 + \dot{z}_2) \\ &= z_1 z_2 - c_1 z_1^2 + \sigma[k_1(z_2 - c_1 z_1) \\ &\quad + A_m(z_2 + \dot{Y}_d - \alpha_1) + B_m U + D - \ddot{Y}_d + \dot{\alpha}_1] \end{aligned} \tag{36}$$

$$\begin{aligned} U &= B_m^{-1} [-k_1(z_2 - c_1 z_1) - A_m(z_2 + \dot{Y}_d - \alpha_1) \\ &\quad - D_{max} \operatorname{sgn}(\sigma) + \ddot{Y}_d - \dot{\alpha}_1 - h(\sigma + \beta \operatorname{sgn}(\sigma))] \end{aligned} \tag{37}$$

where h and β are all positive constants.

Then to integrate the Eqs. (36) and (37). The Eq. (38) is derived, and it can be expressed into matrix of quadratic form as Eq. (39).

$$\begin{aligned} \dot{V}_2 &= -c_1 z_1^2 + z_1 z_2 - h\sigma^2 - h\beta|\sigma| + D\sigma - D_{max}|\sigma| \\ &\leq -c_1 z_1^2 + z_1 z_2 - h\sigma^2 - h\beta|\sigma| + |\sigma|(|D| - D_{max}) \\ &\leq -c_1 z_1^2 + z_1 z_2 - h\sigma^2 - h\beta|\sigma| \end{aligned} \tag{38}$$

$$\dot{V}_2 = -z^T Q z - h\beta|\sigma| \tag{39}$$

where $z = \begin{bmatrix} z_1 \\ z_2 \end{bmatrix}$ and $Q = \begin{bmatrix} c_1 + hk_1^2 & hk_1 - \frac{1}{2} \\ hk_1 - \frac{1}{2} & h \end{bmatrix}$, and Q is a positive definite and symmetric matrix.

In order to comprehend the characteristics of the control variables in the time-varying system, the convergences of Lyapunov function V_2 , and the stability of the control system, it is needed to define an additional function, $w(t)$ as Eq. (40), and take the integral as Eq. (41).

$$w(t) = z^T Q z + h\beta|\sigma| \leq -\dot{V}_2(z_1(t), z_2(t)) \tag{40}$$

$$\int_0^t w(\tau) d\tau \leq V_2(z_1(0), z_2(0)) - V_2(z_1(t), z_2(t)) \tag{41}$$

When the initial value of $V_2(z_1(0), z_2(0))$ is bounded and the $V_2(z_1(t), z_2(t))$ is a non-increasing function, the value of $w(t)$ is bounded as Eq. (42). Simultaneously, $w(t)$ is a continuous function and its differential term $\dot{w}(t)$ is also bounded. According to the Barbalat lemma, it can be inferred that the $w(t)$ converges to zero with time as shown in Eq. (43).

$$\lim_{t \rightarrow \infty} \int_0^t w(\tau) d\tau < \infty \tag{42}$$

$$\lim_{t \rightarrow \infty} w(t) = 0 \tag{43}$$

According to the above equations derivation, it can be deduced that the system variables z_1 and z_2 converge to zero as $t \rightarrow \infty$. It shows that the system control outputs (position y_m and velocity v) converge to the input commands (position y_d and its differential term \dot{y}_d) as Eqs. (44) and (45).

$$\lim_{t \rightarrow \infty} y_m = y_d \tag{44}$$

$$\lim_{t \rightarrow \infty} v = \dot{y}_d \tag{45}$$

Although the system parameters vary and the external interferences impact the control system, the system state variables still convergent stably and asymptotically.

Step 3:

In fact, to estimate the exact values of the external disturbances is difficult in real world. Therefore, the total magnitude of D_{max} is equal to a varying value with time. For this reason, the adaptive law is used to estimate the value of external disturbance D . Firstly, set an equation of estimated error \tilde{D} in disturbance as Eq. (46) and then define the third Lyapunov function V_3 as Eq. (47).

$$\tilde{D} = D - \hat{D} \tag{46}$$

$$V_3 = V_2 + \frac{1}{2\gamma} \tilde{D}^2 \quad (47)$$

where D is the total value of disturbance in real world. \hat{D} is an estimated value of disturbance. And γ is a positive constant.

By taking the derivative of the Lyapunov function V_3 as Eq. (48) and the control input U could be derived as Eq. (49).

$$\begin{aligned} \dot{V}_3 &= \dot{V}_2 - \frac{1}{\gamma} \tilde{D} \dot{\tilde{D}} \\ &= z_1 z_2 - c_1 z_1^2 + \sigma [k_1(z_2 - c_1 z_1) + A_m(z_2 + \dot{Y}_d - \alpha_1) \\ &\quad + B_m U + D - \ddot{Y}_d + \dot{\alpha}_1] - \frac{1}{\gamma} \tilde{D} \dot{\tilde{D}} \\ &= z_1 z_2 - c_1 z_1^2 + \sigma [k_1(z_2 - c_1 z_1) + A_m(z_2 + \dot{Y}_d - \alpha_1) \\ &\quad + B_m U + \hat{D} - \ddot{Y}_d + \dot{\alpha}_1] - \frac{1}{\gamma} \tilde{D} (\dot{\tilde{D}} - \gamma \sigma) \\ U &= B_m^{-1} [-k_1(z_2 - c_1 z_1) - A_m(z_2 + \dot{Y}_d - \alpha_1) \\ &\quad - \hat{D} + \ddot{Y}_d - \dot{\alpha}_1 - h(\sigma + \beta \text{sgn}(\sigma))] \end{aligned} \quad (48) \quad (49)$$

The adaptive law about estimating external disturbances \hat{D} is designed as Eq. (50).

$$\dot{\hat{D}} = \gamma \sigma \quad (50)$$

Finally, to substitute Eqs. (49) and (50) into Eq. (48), Eq. (51) is derived. The matrix Q must be positive and definite as stated in Eq. (52). According to Barbalat lemma, it can infer that $w(t)$ converges to zero with time as Eq. (53).

$$\begin{aligned} \dot{V}_3 &= -c_1 z_1^2 + z_1 z_2 - h\sigma^2 - h\beta|\sigma| \\ &= -z^T Q z - h\beta|\sigma| \\ &= -w(t) \leq 0 \end{aligned} \quad (51)$$

$$|Q| = h(c_1 + hk_1^2) - \left(hk_1 - \frac{1}{2} \right)^2 = h(c_1 + k_1) - \frac{1}{4} > 0 \quad (52)$$

$$\lim_{t \rightarrow \infty} w(t) = 0 \quad (53)$$

Similarly, according to the above equations derivation, it can be deduced that the system variables z_1 and z_2 converge to zero when $t \rightarrow \infty$. This ensures the stability in the control system. Moreover, if the condition is true as Eq. (54) states, the system variables can converge to the sliding surface as shown in Eq. (55).

$$\sigma \dot{\sigma} \leq 0 \quad (54)$$

$$\sigma = 0 \quad (55)$$

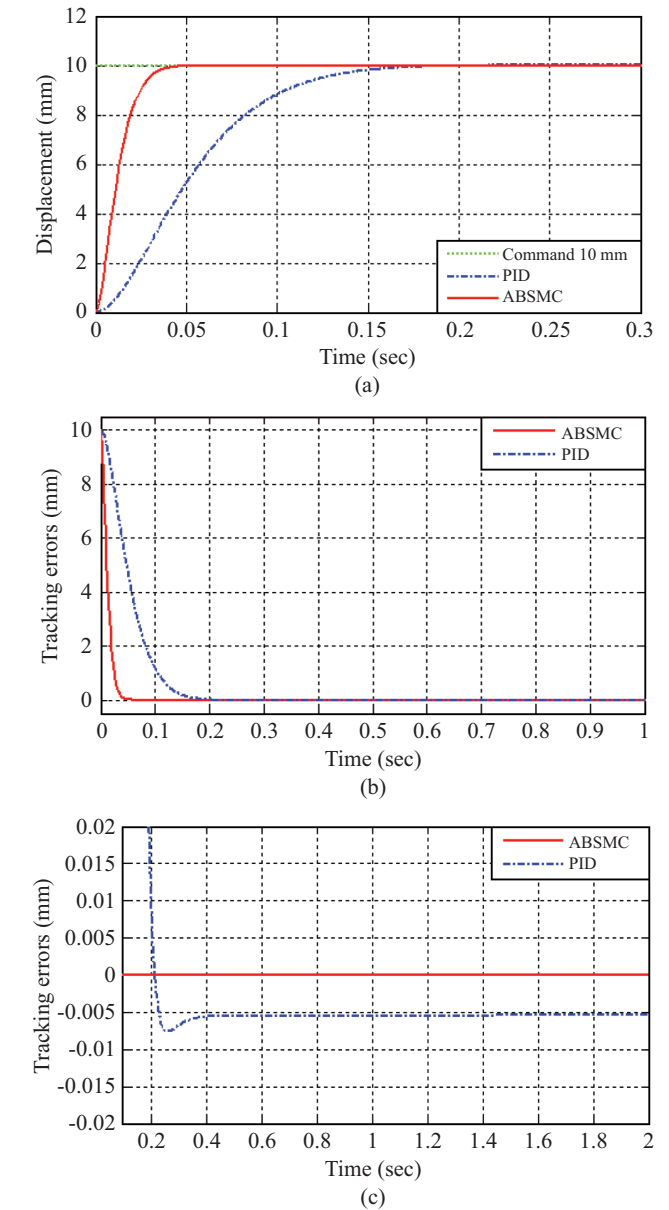


Fig. 7. (a) Step responses 10 mm (simulated results), (b) Tracking errors (simulated results), and (c) Steady state errors (simulated results).

However, the most important of all is that the control input U must be kept in exciting state. It drives the estimated value of the external uncertain disturbances to converge to the real values in the system.

3. The Performance Comparison of PID and ABSMC

The control objects of 10 mm stroke positioning and 10 mm sinusoidal wave dynamical tracking performances are shown as follows.

Case 1: Positioning performances–Step response 10 mm.

The simulation values of the system parameters in PID and ABSMC controllers are given as follows:

PID controller (simulated parameters)

$K_P = 200$	$K_I = 2$	$K_D = 10$
-------------	-----------	------------

ABSMC controller (simulated parameters)

$c_1 = 100$	$k_1 = 50$	$\gamma = 40$
$\beta = 30$	$h = 150$	

The simulation results about step response 10 mm of positioning control, tracking errors, and steady state errors are depicted in Figs. 7(a), (b), and (c).

From the above simulation results of case 1, it is obvious that ABSMC controller has better performances than the PID in positioning control. The rise time of PID and ABSMC are 0.178sec and 0.043sec respectively, and the steady state errors of PID and ABSMC are 5.532 μm and 0.024 μm respectively.

Next, the experiment parameters of the PID and ABSMC are selected as follows.

PID controller (experimental parameters)

$K_P = 0.69$	$K_I = 0.036$	$K_D = 2.95$
--------------	---------------	--------------

ABSMC controller (experimental parameters)

$c_1 = 12$	$k_1 = 15$	$\gamma = 0.2$
$\beta = 15$	$h = 1.5$	

The experimental results about step responses 10 mm of positioning control, tracking errors, and the steady state errors, are depicted in Figs. 8(a), (b), and (c).

From Fig. 8(a), the PID and ABSMC have the transient overshoots, and the percent maximum overshoots of PID and ABSMC are 18.2% and 2.5% respectively. The overshoots can give rise to serious tracking errors and some irregular mechanical vibrations in the transient performances, which impedes the positioning accuracy as Fig. 8(b) shows. Similarly, in the responses of steady state errors in Fig. 8(c), the ABSMC can resist the multiple external disturbances and exhibit good stability and robustness. On the contrary, PID is weak in opposing the external disturbances; its steady state response is easily disturbed.

Case 2: Dynamical tracking performances–Sinusoidal wave response (Amplitude: 10 mm, frequency: 0.5 Hz).

The simulated values of the system parameters of PID and ABSMC controllers are given as follows:

PID controller (simulated parameters)

$K_P = 250$	$K_I = 8$	$K_D = 10$
-------------	-----------	------------

ABSMC controller (simulated parameters)

$c_1 = 90$	$k_1 = 30$	$\gamma = 100$
$\beta = 80$	$h = 115$	

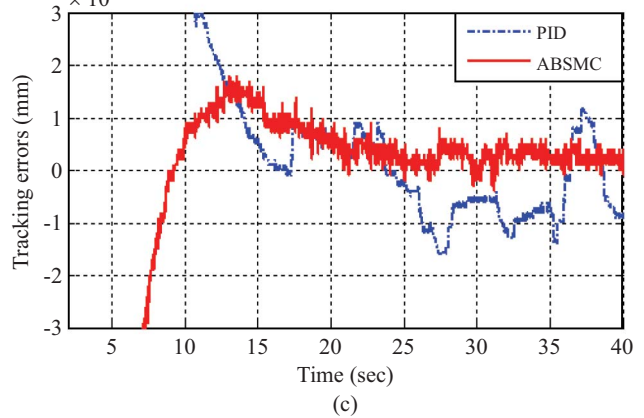
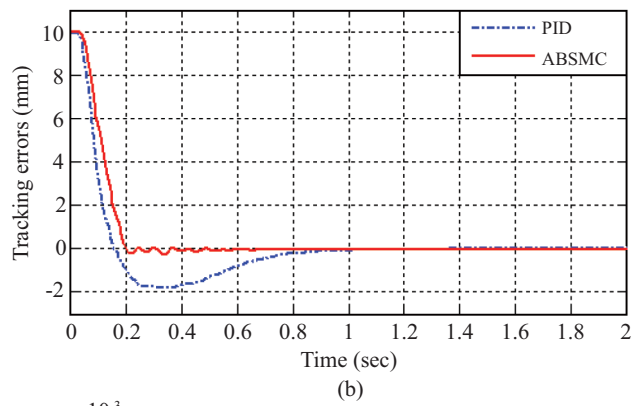
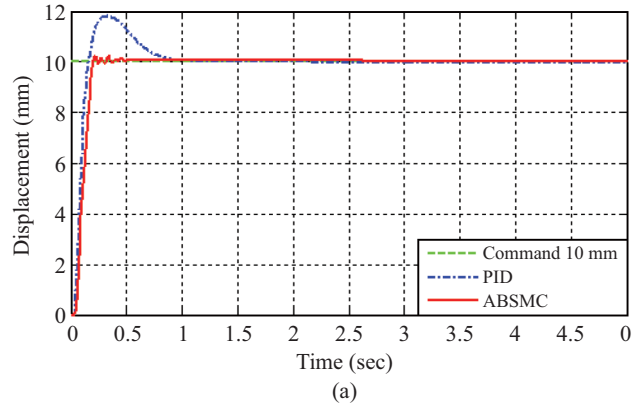


Fig. 8. (a) Step responses 10 mm (experimental results), (b) Tracking errors (experimental results), and (c) Steady state errors (experimental results).

The simulation results in sinusoidal wave responses of dynamical tracking control, and tracking errors are depicted in Figs. 9(a) and (b).

In the simulated results shown in Fig. 9, ABSMC has excellent performances in dynamical tracking control, whereas the tracking errors of the PID are not only larger than ABSMC but also reached maximum at the inflection points in sinusoidal wave responses. The maximum tracking errors of PID and ABSMC are 0.148 mm and 0.011 mm respectively.

Moreover, the experiment parameters of the PID and ABSMC are selected as follows:

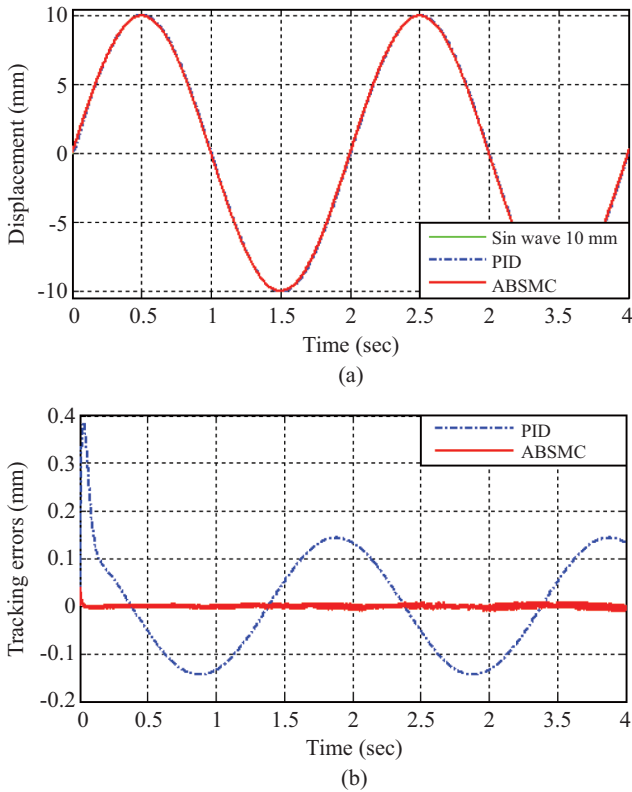


Fig. 9. (a) Sin wave responses (simulated results) and (b) Tracking errors (simulated results).

PID controller (experimental parameters)

$K_p = 0.69$	$K_I = 0.036$	$K_D = 2.95$
--------------	---------------	--------------

ABSMC controller (experimental parameters)

$c_1 = 12$	$k_1 = 15$	$\gamma = 0.2$
$\beta = 15$	$h = 1.5$	

The experimental results about sinusoidal wave responses of dynamical tracking control and tracking errors are depicted in Figs. 10(a), (b), (c) and (d).

The experimental results show that the ABSMC has better abilities to restrain the disturbances of friction force and also has the abilities to suppress the ripple effect.

In the sinusoidal wave tracking responses, PID exhibits significant tracking errors during transient state in Figs. 10(a) and (b). The time points of PID and ABSMC which the tracking errors are less than 0.5 mm are 0.585 sec and 0.283 sec, respectively (Fig. 10(c)). The values of the maximum tracking errors of PID and ABSMC are 1.76 mm and 0.94 mm at transient state. Moreover, the tracking errors of PID and ABSMC are 0.39 mm and 0.13 mm (RMS) (Fig. 10(d)). Therefore, the ABSMC has the preferable transient responses and more accurate controlled precision in position control.

4. The Controller Design Process of VSC

After designing the controllers of PID and ABSMC and analyzing their responses, the performances of transient state

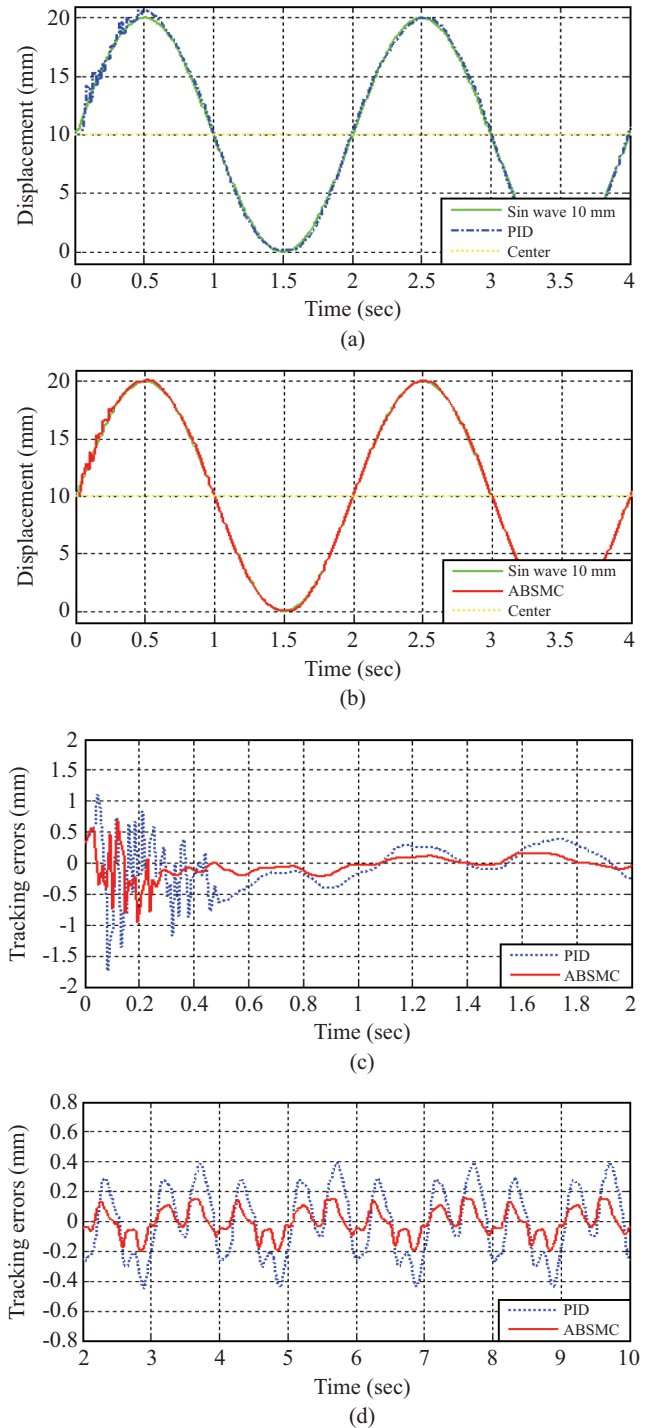


Fig. 10. (a) Sine wave response of PID (experimental results), (b) Sine wave response of ABSMC (experimental results), (c) Transient state tracking errors (experimental results), and (d) Tracking errors (experimental results).

responses are still undesirable even when the performances of ABSMC are found to be better than PID.

The design of controllers of PID and ABSMC and the analysis of their responses, the performances of transient state responses are still undesirable even when the performances of

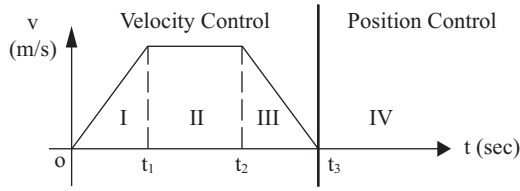


Fig. 11. The variable speed curve.

ABSMC are found to be better than PID. The oversize acceleration and velocity of linear motor make some unnecessary overshoots and mechanical vibrations in transient responses, which seriously disturb the control performances. Therefore, the speed controller VSC is proposed to improve the tracking errors during transient state responses [11, 13].

The VSC shows better transient responses in positioning control which suppresses the mechanism vibrations and overshoots at initial derivation. In addition VSC can also be applied with variable speed principles to switch the velocity control mode into the position control mode.

The velocity control mode is divided into three segments, the constant acceleration, the uniform velocity, and the constant deceleration. The segments of the variable speed curve are shown in Fig. 11.

The variable speed sliding mode functions S_n of each segment I, II, and III are shown in Eq. (56).

$$\begin{cases} S_I = x_1 - \frac{1}{2\alpha_1} x_2^2 - x_0 = 0 \\ S_{II} = x_2 - v_m = 0 \\ S_{III} = x_1 + \frac{1}{2\alpha_2} x_2^2 = 0 \end{cases} \quad (56)$$

where x_0 is the initial displacement, x_1 is the error of displacement, x_2 is the mover velocity, α_1 is the acceleration of region I, α_2 is the deceleration of region III, and v_m is the uniform velocity of region II.

As a result of the above mentioned, there are a lot of external disturbances in the control system. Therefore, to ensure the convergence of system states, variable speed sliding surface S_n is important. According to the Lyapunov lemma theory, if the controlled system satisfies the sliding condition as Eq. (57) states, then the sliding mode, $S_n = 0$ exists. It can therefore define the system input as Eq. (58) to ensure the stability in VSC and the system state variables converge to the equilibrium points.

$$S_n \cdot \dot{S}_n < 0 \quad (57)$$

$$F_e = K_t \cdot U = K_t (h_1 + h_2 x_2) \quad (58)$$

where h_1 and h_2 are the system parameters and the values are selected based on the system performance requirements.

Table 1. The system hardware parameters.

Mass	12 Kg
Peak Force	679 N
Continuous force	339 N
Force constant	68.5894 N/A _{rms}
Back emf constant	51 V _{rms} /m/s
Electrical time constant	10.3 ms
Resistance	6.2 ohms
Inductance	64 mH
Thermal resistance	0.66°C/W
Magnetic pole pair length	32 mm
Velocity Limit	200 mm/s



Fig. 12. The PMLSM positioning platform system.

IV. EXPERIMENTAL RESULTS

1. The Experimental Equipment

In this research, the positioning platform utilizes the permanent magnet iron core linear synchronous motor (PMLSM) as the driving equipment (model number LMS27, HIWIN Corp., Taiwan). The effective stroke of the PMLSM is 200 mm. The hard structures of PMLSM positioning platform system are shown in Fig. 12.

The model number of the optical linear encoder is RGH22Y30D61, RENISHAW Corp., UK. Its highest accuracy of resolution is 100 nm. The power driver (model number 800-1519A, COPLEY, Inc., USA) in our system is to provide sufficient current to induce the electromagnetic force. The embedded microbox used in this research is PXIe-1062Q manufactured by National Instruments Inc., USA, and the multifunction data acquisition (DAQ) devices is model PXIe-6363, which are manufactured by National Instruments Inc., USA. The clock rate of DAQ is 1.73G Hz, which allows us to accomplish real-time control in implementation. Moreover, the controller design software is Labview 2010, which supports the functions of PC-based control and graphical human-machine interface in the design processes. It is also manufactured by National Instruments Inc., USA.

Above all the hardware structures parameters of PMLSM are listed in Table 1.

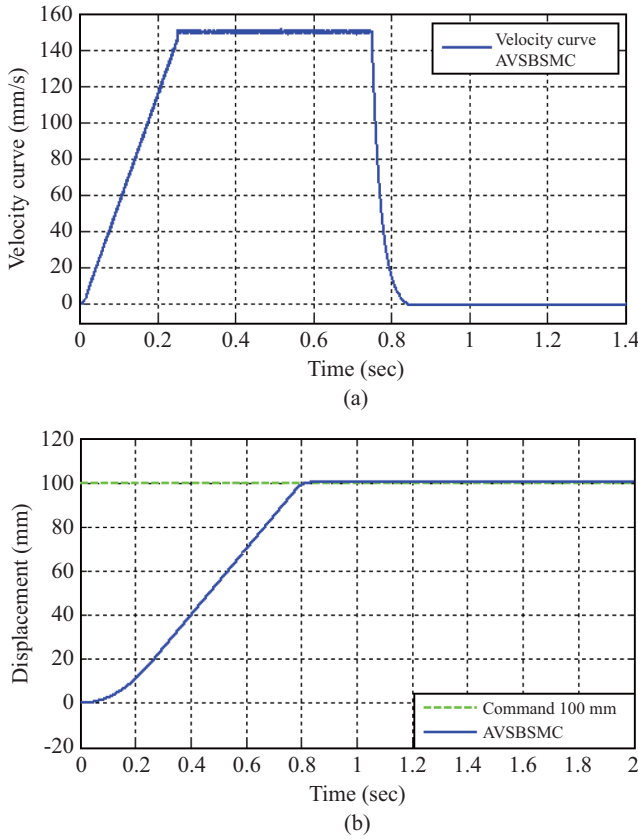


Fig. 13. (a) Velocity curve (simulated results) and (b) Step responses 100 mm (simulated results).

2. The Simulated Results and Experimental Results

In this research, the positioning performances of the step responses 100 mm are used to compare the positioning efficiency between ABSMC and AVSBSMC.

In order to realize the control performances, feasibilities, and stability in positioning control of AVSBSMC controller prior the experiments software MATLAB R2008a was used to simulate the system responses of AVSBSMC. The control object serves to execute positioning control obeying the trapezoidal velocity profile with $\alpha_1 = 600 \text{ mm/s}^2$, $v_m = 150 \text{ mm/s}$, $\alpha_2 = 1875 \text{ mm/s}^2$, $t_1 = 0.25 \text{ sec}$, $t_2 = 0.75 \text{ sec}$, and $t_3 = 0.83 \text{ sec}$ in addition, the system parameters of control gains h_1 and h_2 are set as $\delta_1 = 20$, $\zeta_1 = 20$, $\delta_2 = 15$, $\zeta_2 = 12$, $\delta_3 = 25$, $\zeta_3 = 25$, and $x_0 = 0$ in the velocity control mode. The parameters of ABSMC are set as $c_1 = 100$, $k_1 = 50$, $\gamma = 40$, $\beta = 30$, and $h = 150$ in position control mode. The simulation results about the variable velocity curve and the step response 100 mm of AVSBSMC are depicted in Figs. 13(a) and (b).

From the simulation results, it is obvious that the AVSBSMC controller has better performance at transient response over ABSMC with the ability to suppresses transient overshoot effectively as well as supplying desirable motor velocity values [12, 14].

In the experiment, a software Labview 2010 was used to

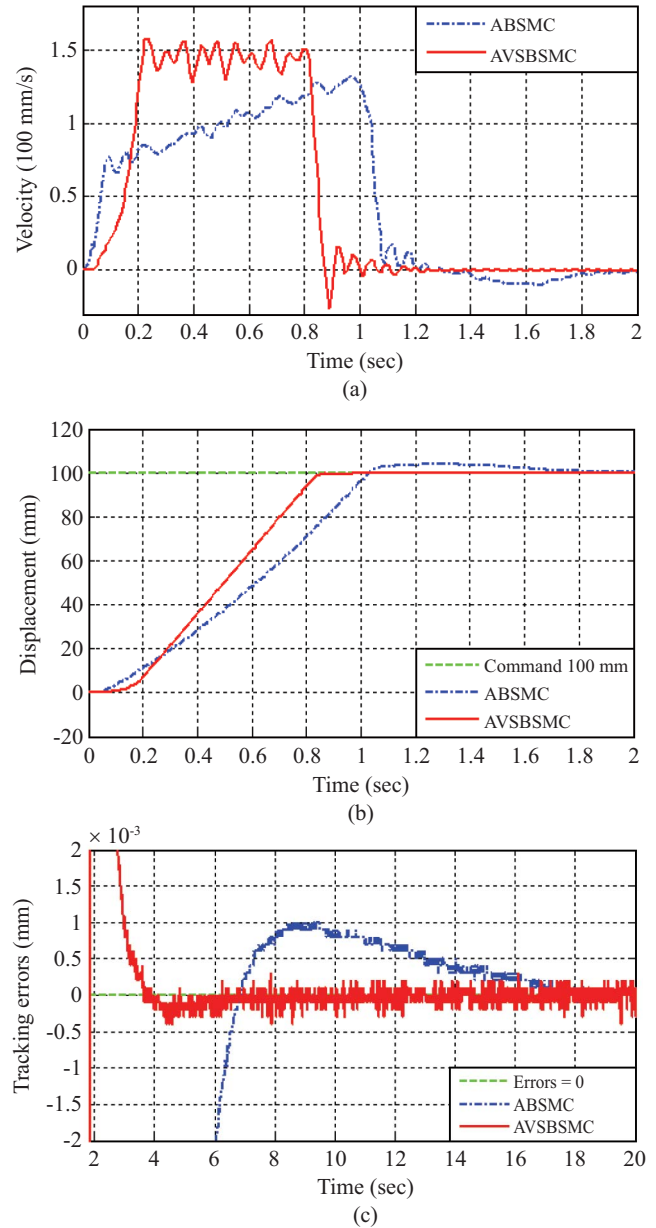


Fig. 14. (a) Velocity curve (experimental results), (b) Step responses 100 mm (experimental results), and (c) Tracking errors (experimental results).

design the application programming interface (API) in the system controllers, and to control PMLSM.

The system parameters of control gains h_1 and h_2 are set as $\delta_1 = 1$, $\zeta_1 = 3$, $\delta_2 = 0.5$, $\zeta_2 = 2.5$, $\delta_3 = 1$, $\zeta_3 = 3$, and $x_0 = 0$ in velocity control mode. The parameters of ABSMC are set as $c_1 = 8.5$, $k_1 = 8.5$, $\gamma = 1.25$, $\beta = 3.75$, and $h = 1.25$ in position control mode. The experimental results about the variable velocity curves, the step responses 100 mm, and tracking errors of our control scheme are shown in Figs. 14(a) to (c).

According to Fig. 14(a), the velocity curve of AVSBSMC is trapezoidal and its results are very close to simulation results in Fig. 13(a). However, the velocity curve of ABSMC belongs to

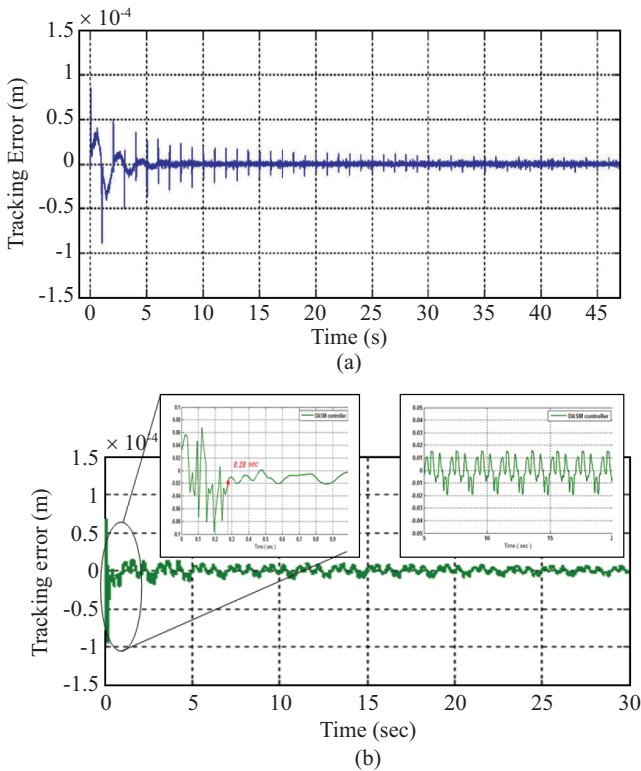


Fig. 15. (a) The tracking response of MPC controller and (b) The tracking response of AVSBSMC controller.

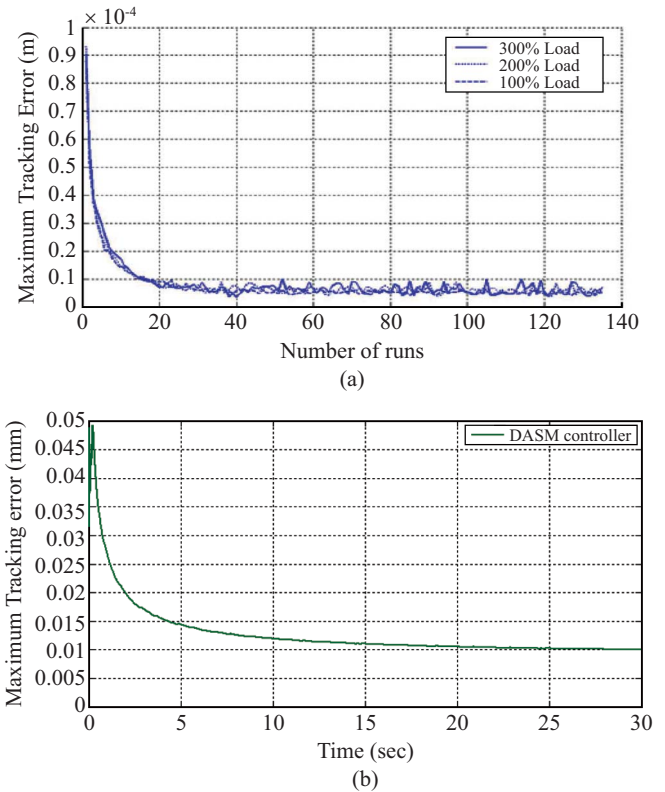


Fig. 16. (a) The tracking error convergence of MPC controller and (b) The tracking error convergence of AVSBSMC controller.

to an irregular polygonal curve. Thus, the system is inclined to bring more excess transient overshoots and positioning errors.

The external disturbances and other noises destroy the smoothness of the PMLSM velocity curve of AVSBSMC shown in Fig. 14(a), and these interferences are also the sources of positioning errors. Fortunately, these positioning errors are smaller than VSC control and can be compensated rapidly by ABSMC in position control mode. Relative to the ABSMC without VSC controller, the converged speed of compensating the positioning errors is slower than AVSBSMC as shown in Fig. 14(c).

Finally, it is obvious that the transient overshoots of step response 100 mm can be eliminated successfully in AVSBSMC as shown in Fig. 14(b). Correspondingly, the ABSMC still has the bigger transient overshoots. Hence, this composited controller can improve the transient performance effectively and promote the compensation of errors rapidly in the positioning system [9, 15].

3. Comparison of System Performance

To enhance AVSBSMC control in testing the relative positioning performance, we made a comparison between hereby developed controller with Cao and Low's research [3] which used a model predictive control (MPC) approach for linear motor. The reference input was set as a sinusoidal motion with amplitude 10 mm and 0.5 Hz. Some results are shown below:

- (1) AVSBSMC and MPC controllers have the same motion trajectories, but load weights of these two carriers were different: AVSBSMC: 12 kg, and MPC: 2.6 kg.
- (2) Fig. 15(a) shows the setting time, 4 sec for the MPC controller and Fig. 15(b) shows the setting time of 0.28 sec for the AVSBSMC controller.
- (3) Figs. 16(a) and (b) show the tracking error converged times. The time of steady state tracking response was 27.56 sec for AVSBSMC controller and 40 sec for RMPC controller when the maximum error was reduced to less than 1 μm .
- (4) Parts of the steady state errors, the steady state error of AVSBSMC (load weight 12 kg) was 13 μm and those of RMPC (load weight 2.6, 5.2 and 7.8 kg) were 8.5, 9.2 and 9.8 μm .

The results of total comparisons are shown in Table 2. Based on these results; the AVSBSMC controller was shown to have a better transient response and a more suitable steady state response than MPC. Therefore, the developed AVSBSMC controller can effectively solve the coupling problem in this research.

V. CONCLUSION

In this research, two controllers are designed, ABSMC, and

Table 2. Comparison of system performance with hereby developed controller and Cao [3].

Item	AVSBSMC controller (hereby developed)	MPC controller (R. Cao and K. S. Low)
Load weight (carrier)	12 kg	2.6 kg
Transient response (Tracking error less than 20 μm of time)	0.28 sec	\approx 4 sec
Steady state response of time	27.56 sec	\approx 40 sec (20 runs)
Steady state response (steady error)	Load 12 kg \approx 13 μm	Load 2.6 kg \approx 8.5 μm
		Load 5.2 kg \approx 9.2 μm
		Load 7.8 kg \approx 9.8 μm

VSC. By combining ABSMC with VSC, AVSBSMC is derived. The experimental results show that AVSBSMC controller has an excellent ability of high precision positioning control. The experimental data of step response of 100 mm also shows that, the control precision class which we can implement is about 0.13 μm in precision positioning. As to the amount of transient overshoot, its suppression to less than 1% of 100 mm can be achieved. Therefore, this proposed control scheme of AVSBSMC is shown to be an outstanding controller in a high precision positioning system.

REFERENCES

- Bianchini, C., Immovilli, F., Cocconcelli, M., Rubini, R., and Bellini, A., "Fault detection of linear bearings in brushless ac linear motors by vibration analysis," *IEEE Transactions on Industrial Electronics*, Vol. 58, No. 5, pp. 1684-1694 (2011).
- Butcher, M. and Karimi, A., "Linear parameter-varying iterative learning control with application to a linear motor system," *IEEE/ASME Transactions on Mechatronics*, Vol. 15, No. 3, pp. 412-420 (2010).
- Cao, R. and Low, K. S., "A repetitive model predictive control approach for precision tracking of a linear motion system," *IEEE Transactions on Industrial Electronics*, Vol. 56, No. 6, pp. 1955-1962 (2009).
- Chang, Y. C., *Design and Implementation of CMAC-Based Controller for Permanent Magnet Linear Synchronous Motor Drive*, Master Thesis, Tatung University, Taipei, Taiwan (2003).
- Chen, S. L., Tan, K. K., Huang, S., and Teo, C. S., "Modeling and compensation of ripples and friction in permanent-magnet linear motor using a hysteretic relay," *IEEE/ASME Transactions on Mechatronics*, Vol. 15, No. 4, pp. 586-594 (2010).
- Cupertino, F., Naso, D., Mininno, E., and Turchiano, B., "Sliding-mode control with double boundary layer for robust compensation of payload mass and friction in linear motors," *IEEE Transactions on Industry Applications*, Vol. 45, No. 5, pp. 1688-1696 (2009).
- Famouri, P., "Control of a linear permanent magnet brushless dc motor via exact linearization methods," *IEEE Transactions on Energy Conversion*, Vol. 7, No. 3, pp. 544-551 (1992).
- Lin, F. J., Chang, C. K., and Huang, P. K., "FPGA-based adaptive backstepping sliding-mode control for linear induction motor drive," *IEEE Transactions on Power Electronics*, Vol. 22, No. 4, pp. 1222-1231 (2007).
- Lin, F. J., Chou, P. H., Chen, C. S., and Lin, Y. S., "DSP-based cross-coupled synchronous control for dual linear motors via intelligent complementary sliding mode control," *IEEE Transactions on Industrial Electronics*, Vol. 59, No. 2, pp. 1061-1073 (2012).
- Lin, F. J., Shen, P. H., and Hsu, S. P., "Adaptive backstepping sliding mode control for linear induction motor drive," *IEE Proceedings - Electric Power Applications*, Vol. 149, No. 3, pp. 184-194 (2002).
- Lin, F. J., Shyu, K. K., and Lin, C. H., "Incremental motion control of linear synchronous motor," *IEEE Transactions on Aerospace and Electronic Systems*, Vol. 38, No. 3, pp. 1011-1022 (2002).
- Liu, T. H., Lee, Y. C., and Chang, Y. H., "Adaptive controller design for a linear motor control system," *IEEE Transactions on Aerospace and Electronic Systems*, Vol. 40, No. 2, pp. 601-616 (2004).
- Shyu, K. K. and Lai, C. K., "Incremental motion control of synchronous reluctance motor via multi-segment sliding mode control method," *IEEE Transactions on Control Systems Technology*, Vol. 10, No. 2, pp. 169-176 (2002).
- Wu, J., Xiong, Z., Lee, K. M., and Ding, H., "High-acceleration precision point-to-point motion control with look-ahead properties," *IEEE Transactions on Industrial Electronics*, Vol. 58, No. 9, pp. 4343-4352 (2011).
- Zhang, Y., Shieh, L. S., and Dunn, A. C., "PID controller design for disturbed multivariable systems," *IEE Proceedings - Control Theory Applications*, Vol. 151, No. 5, pp. 567-576 (2004).
- Zschaecck, S., Amthor, A., and Ament, C., "Decentralized high precision motion control for nanopositioning and nanomeasuring machines," *IECON 2011 - 37th Annual Conference on IEEE Industrial Electronics Society*, pp. 546-551 (2011).